M. A. Gevelber
Manufacturing Engineering Department,
College of Engineering,
Boston University,
Boston, MA 02215

G. Stephanopoulos
Department of Chemical Engineering,
Massachusetts Institute of Technology,
Cambridge, MA 02139

Modeling and Dynamic Characterization of the Czochralski Crystal Growth Process

A lumped parameter model of the Czochralski crystal growth process is proposed that captures the dominant nonlinear dynamics, internal coupling, and disturbance structure. Conventional and advanced actuators are modeled. The dynamic characteristics of the interface shape and input/outputs that limit the achievable controller performance are identified.

1 Introduction

In previous papers we reported a 7th order lumped model of the process with a flat interface (Gevelber and Stephanopoulos, 1987 and Gevelber et al., 1988). In this paper, a more detailed low order model is presented that approximates the interface shape and local temperature gradients. Additional inputs such as bottom heater, magnetic field, and a heater near the meniscus are also included in order to determine their relative performance. The interface low order model (ILOM) will be used to determine the dominant dynamics of the interface and system and to evaluate alternative inputs, outputs, and control structure designs. A companion paper presents an analysis of the control requirements and a performance evaluation of a new control structure.

A schematic of the Czochralski process is shown in Fig. 1. The molten material referred to as the melt, is contained in a quartz crucible that is supported by a graphite susceptor. Heat can be supplied by graphite heaters that surround the crucible, although RF heaters and heat pipes have also been used. The ILOM is based on a commercial system with an electrical resistance heater that uses between 20 to 30 kW of power. Most of this power, however, does not pass through the crystal. The entire system is contained in metal vessel which can either be evacuated or pressurized with different gases.

The crystal is begun by bringing a small seed in contact with the melt. After some equilibration time, the seed is pulled away from the melt. The crystal acts as a "cooling fin" which drives the solidification process. The operator adjusts the pulling rate and heater power to first neck the crystal which is a long thin section used to grow out dislocations that might be propagated into the crystal during seeding. The crystal is then grown out to diameter, shouldered, and maintained at the desired diameter. As the crystal grows in length, the melt level decreases, and the operator or automatic control system adjusts the power and/or pull rate to maintain constant diameter. Towards the end of growth run, the crystal can be tapered into a tail or suddenly lifted up from the melt to end the growth run.

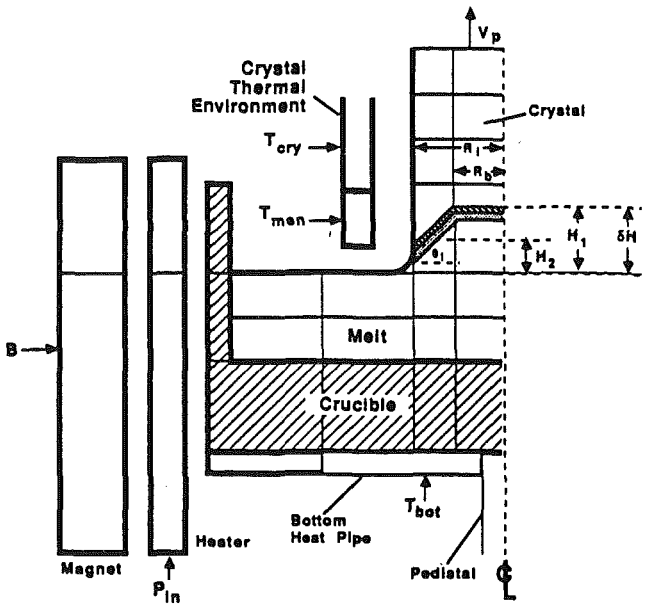

Fig. 1 Czochralski system schematic for ILOM

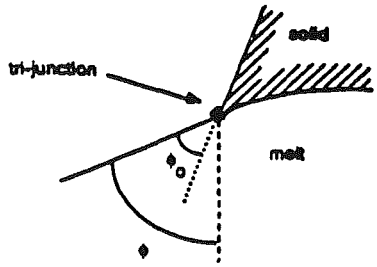

Fig. 2 Interface region schematic

Figure 2 shows the boundary region between the liquid and solid phases. The melt surface attaches to the solid at a level above the melt. This liquid area is called the meniscus. The angle at which the liquid attaches to the solid is denoted ϕ and depends on the crystal radius, R_i, interface height, H_i, the melt surface tension, as well as other material properties. The shape

Contributed by the Dynamic Systems and Control Division for publication in the JOURNAL OF DYNAMIC SYSTEMS, MEASUREMENT, AND CONTROL. Manuscript received by the Dynamic Systems and Control Division February 24, 1989; revised manuscript received August 26, 1991. Associate Technical Editor: A. G. Ulsoy.

of the solid/liquid interface is typically nonplaner, reflecting the local heat transfer conditions within the crystal and of the crystal and melt surfaces. The interface shape is important since it indicates the ratio between the local radial and axial temperature gradients and also since it affects the local fluid flow and mass transport. The deflection between the center and edge, denoted δH, and the angle at which the interface makes at the surface with respect to the horizontal, denoted θ_i, can be used to parameterize the interface shape (Fig. 1).

Only limited attention has been given to analyzing the dynamics of the process. Robertson and Young (1975) reported on the ability to grow germanium crystals without any adjustment to input parameters of pull rate or heater power, showing that the system can be operated in a quasi-steady state. Steel and Hill (1975) developed a lumped model assuming a flat interface, which predicted a dominant pair of underdamped poles. Gevelber and Stephanopoulos (1987) presented a lumped model assuming a flat interface that directly included heater and pull rate inputs. This model predicted that a real pole dominated the response, although the variation of the pole/zero structure was shown to be dependent on the operating regime. They also identified important process disturbances related to the changing melt level (Gevelber et al., 1988). Hurle et al. (1986) conducted an experimental system identification on a growing crystal, verifying the overdamped interface dynamics, the inherent stability of the interface, and the right half plane (RHP) zero of the weight measurement. The RHP zero affect can also be seen in Juhasz and Szabo's data (1986).

Borodin et al. (1979) experimentally determined the interface shapes for NaCl and used an axisymmetric conduction model of the crystal to determine the crystal thermal gradients. They concluded that concave and convex interface shapes have distinctly different axial temperature gradients which is important for thermal stress. Srivastava et al. (1985) developed a steady-state model which was used to gain insight into the relation between inputs and interface shape. However, it neglects important dynamic considerations important for control. Derby and Brown (1986) developed a detailed steady-state and dynamic model of the complete Czochralski system. Early work used a conduction dominated representation of the melt, although a steady state fluid model has been developed (Sackinger, 1988).

2 Modeling

The ILOM consists of 28 lumped thermal elements to account for thermal gradients in the system (10 for the melt, 8 for the crystal, 2 each for the heater and shield, and 6 for the crucible) and 10 auxiliary state equations that relate the geometric deformation of the melt level decrease and crystal elements (Fig. 1). A fourth order Runge-Kutta scheme is used to numerically integrate the nonlinear equations, while a first order central difference technique is used to determine the system, input, and output Jacobians used in the eigenstructure and singular value decomposition (SVD) analyses.

2.1 Heater, Crucible, Melt and Crystal. The heater and shield are each modeled with two lumped elements that are internally coupled by conduction heat transfer. The vertical length in the two regions of each component are time varying, where the boundary is matched to the melt height. The reason for this is to reflect the changing heat transfer in the crucible due to the increase in exposed inner crucible wall as the melt height decreases. The side of the crucible (which includes the graphite support) is modelled as two cylindrical elements whose height varies with the melt height. The bottom of the crucible is modelled as thick graphite, reflecting the design of conventional pullers. The graphite crucible bottom is spatially lumped into four elements that correspond to the melt discretization. Each bottom crucible element is connected to a temperature source to reflect the typical loss out the crucible bottom to thermal sinks such as the bottom of the chamber and the water cooled support shaft. To investigate alternative designs, the crucible bottom can also be set to reflect either an adiabatic condition (i.e., perfectly insulated), or active bottom heaters which can be used to control the melt temperature and/or interface shape. The thermal sources are assumed to be a uniform temperature, T_{bot}, which could be achieved by the use of a heat pipe.

Different environmental temperatures are used to reflect the different thermal sinks in the system. T_e is the sink that the shield radiates to and corresponds to the jacket of the growth system. The thermal sink at the top of the system is T_{me}, which exchanges heat with the melt surface and the inner crucible wall.

The melt is discretized to resolve the radial and vertical components of heat flow in the melt and the effects of the different heat sources and sinks. Heat transfer from the crucible wall to the melt occurs both from contact with the crucible side and from radiation from the exposed inner crucible surface. Heat transfer within the melt is modeled as conduction, which approximates the situation when a strong magnetic field on the order of 2 kilogauss is applied (Tangborn, 1987 and Sackinger, 1988).

The size of the thermal elements are time varying, reflecting the change in the melt height and changes in interface shape. The thermal state equations for each lumped thermal element has the form:

$$m_j c_j \dot{T}_j = \sum_i Q_{i,j} - \dot{m}_j c_j T_j \tag{1}$$

where m_j is the mass of the lumped element j, c_j is the specific heat of the material, $Q_{i,j}$ is the positive heat flux into the jth element from the ith element, and T_j is the element temperature.

The crystal is divided into an inner core and an outer annulus and into four different vertical regions. These vertical segments determine the crystal heat fluxes Q_{x1}, Q_{x2} at the interface. Two axial segments are used within the first R_i of the crystal length in order to capture the local heat transfer effect on the interface shape.

A heat pipe is assumed to surround the crystal with temperature T_{cry}, serving as the thermal sink. Use of such a heat pipe was proposed by Jasinski and Witt (1986) and is advantageous since: (a) it eliminates the batch disturbance effect of the crystal being exposed to the time varying thermal environment (Gevelber et al., 1988), (b) it or other controllable thermal sources, can be used to maintain the crystal temper-

Nomenclature

H_i = interface height
LOM = low order model
MIMO = multiple-input-multiple-output
P_{in} = heater power
Q_h = heat of fusion flux
Q_i = melt-interface heat flux
Q_x = crystal-environment heat flux
R_b = radius of boundary at inner/outer interface segment
R_i = crystal interface radius
RHP = right half plane
SISO = single-input-single-output
$\mathbf{u}$ = input vector
V_p = pulling rate
$\mathbf{y}$ = output vector
δH = interface deflection
$\delta\mathbf{y}$ = output error vector
$\partial T/\partial r$ = radial temperature gradient
$\partial T/\partial z$ = axial temperature gradient
θ_i = interface angle
κ_2 = euclidean condition number

ature gradients at levels required to meet the thermal stress limits (Jasinski and Witt, 1986 and Motakef, 1989), (*c*) it provides an additional actuator for use in interface shape control and (*d*) it maintains an axisymmetric thermal field. In practice, industrial companies have also been seen to utilize additional controllable heaters (Cambridge, 1986) although none yet offer one that surrounds the crystal.

The geometric state equations that describe the radial changes in the crystal lumped elements are of the form:

$$\dot{R}_j = \frac{1}{\tau_j}(-R_j + R_{j-1}) \tag{2}$$

$$\tau_j = \frac{1/2\,\ell_j}{V_p} \tag{3}$$

where R_{j-1} is the radius of the element below the jth element and ℓ_j is the length of the element. This time lag equation represents the physical time it takes for the radius changes to propagate due to how fast the crystal is being pulled.

The length of the top elements changes to reflect the increase in crystal length. The lengthening of the crystal increases the crystal's effective heat transfer area and causes the crystal interface to experience a changing heat flux.

2.2 Interface Equations. Four states are used to approximate the dynamics of the interface. These states correspond to the diameters (R_i, R_b) and heights (H_1, H_2) of an inner and outer interface elements (Fig. 1). The interface shape is modeled as being piecewise linear, so therefore, the interface height velocity is also piecewise linear. The local radial and axial temperature gradients in the elements surrounding the outer interface element are used to determine the interface slope, while a heat balance is performed to derive the interface height state equations for both regions.

The time derivative of the outer region's interface height as a function of radius is:

$$\dot{H}_2 = \dot{H}_1 + (\dot{H}_{2c} - \dot{H}_1)\left(\frac{r - R_b}{R_{2c} - R_b}\right) \tag{4}$$

where H_{2c} is the height at the center of the outer segment, $r = R_{2c} = 0.5(R_b + R_i)$.

The state equation for the center height, H_{2c}, of the outer region is derived from the heat balance for the outer annulus which is: given by $Q_{x,2} = Q_{h,2} + Q_{i,2}$ where $Q_{x,2}$ is the crystal heat flux, $Q_{h,2}$ is the heat of fusion released, and $Q_{i,2}$ is the heat flux from the melt into the interface all for the outer segment. $Q_{h,2}$ is related to the local growth rate by:

$$Q_{h,2} = 2\pi \int_{R_b}^{R_i} r(V_p - \dot{H}_2(r))\,dr \tag{5}$$

The integral of Eq. (5) is evaluated using Eq. (4), and then rearranged to obtain an expression for H_{2c}.

The inner region is assured to have a flat horizontal interface shape, since an axisymmetric thermal environment must have zero radial gradient at the center. The inner region is characterized by two state variables: the outer edge of the region, R_b and the interface height above the melt level, H_1. Taking a heat balance about the inner region (similar to the derivation provided in Appendix E of Gevelber and Stephanopoulos, 1987) and solving in terms of $\dot{H}_1$ yields:

$$\dot{H}_1 = V_p - \dot{H}_m - \frac{Q_{x,1} - Q_{i,1}}{H_f \rho_s \pi R_b^2} \tag{6}$$

where $Q_{x,1}$ and $Q_{i,1}$ are the heat fluxes related to the inner interface segment.

The state equation for the crystal diameter, R_i is

$$\dot{R}_i = \frac{Q_{x,t} - Q_{i,t}}{H_f \rho_s \pi R_i^2} \tan(\phi - \phi_0) \tag{7}$$

where $Q_{x,t} = Q_{x1} + Q_{x2}$, $Q_{i,t} = Q_{i,1} + Q_{i,2}$. This equation is derived from a mass balance about the interface (see Appendix C of Gevelber and Stephanopoulos, 1987). The relation of the crystal radius to the meniscus wetting angle, ϕ is shown in Fig. 2. When the wetting angle equals the equilibrium angle, ϕ_o, the crystal is growing straight, while if $\phi > \phi_0$, the radius is increasing. The meniscus angle ϕ, which is a function of R_i and H_i, algebraically couples Eqs. (6) and (8). The meniscus shape, which is obtained by solving for the equilibrium condition of Laplace-Young equation, is given by an algebraic fit in terms of ϕ to R_i and H_i (see Appendix B in Gevelber and Stephanopoulos, 1987).

The inner boundary radius R_b is determined by finding the intersection between the two regions. The average slope in the outer region is given by:

$$\bar{\theta}_i = \tan^{-1}\frac{(\partial T/\partial r)_{\text{avg}}}{(\partial T/\partial z)_{\text{avg}}} \tag{8}$$

where $(\partial T/\partial r)_{\text{avg}}$, and $(\partial T/\partial z)_{\text{avg}}$ are the average radial and axial temperature gradients in the outer annulus which are calculated from the temperature states of the model. Since the intersection does not change instantaneously, a first order lag equation is used to determine the change of R_b where the time constant is taken to be a function of the pulling rate.

2.3 Alternative Inputs. The inputs that are represented in the ILOM include: the conventional inputs of pull rate, V_p, and main melt heaters, P_{in}, as well as actuators that have recently been introduced such as bottom heatpipe, T_{bot}, heatpipe near the meniscus, T_{men}, heat pipe that surrounds the crystal, T_{cry}, and application of a magnetic field, B. This section provides the modeling assumptions related to the non-conventional inputs.

Bottom heaters are now being offered by commercial puller vendors. For systems without a thermal environment that decouples the crucible from the crystal, the bottom heater provides a way of heating the melt without directly increasing the temperature of the exposed sides of the crucible. The intent is to minimize the effect on the crystal gradients. Thus, the bottom heater could be used to compensate for the batch disturbance effects without directly affecting the crystal gradients.

There have been a variety of different proposals for using thermal actuators placed near the interface region including cooling jets, infrared heaters, and heat pipes (Brice, 1971; Ekhult and Carlberg, 1986; Jasinski and Witt, 1986). In the ILOM, such thermal actuators are modelled as isothermal sources that can interact only with the meniscus and the local crystal surface above the triple-point. As such, these actuators can also serve as sinks to remove heat from the interface area.

The magnetic field is modelled parametrically by using an effective thermal conduction coefficient. In the limit of 2 kilogauss magnetic field, both modeling (Tangborn, 1987 and Sackinger, 1988) and experiments (Kobayashi, 1986) have shown that the melt heat transfer becomes conduction dominated which is the condition assumed in the ILOM. To study the effectiveness of the magnetic field as an actuator, a scaling between the magnetic field and the effective melt conductance is derived from data obtained during a growth run at M.I.T. by Xue Zhong Cao. Cao observed that when the magnetic field is ramped between zero field and 2500 gauss, that the heater temperature needed to be changed by 50 K in order to keep the crystal seed at the same diameter. The scaling used in the ILOM is obtained by determining the change in melt conductivity that is needed to reproduce the heater temperature change.

3 Dynamic Characterization

It is important to develop an understanding of the dynamic features of the inputs, outputs, and system, as well as the effects and structure of the disturbances. The nonlinear model is linearized (Table 1) at a characteristic operating point of

Table 1 Dominant time constants for the ILOM

$\tau_{real} = 2172$ s.
$\tau_{real} = 821$ s.
$\tau_{real} = 399$ s.
$\tau_{real} = 232$ s.
$\tau_{real} = 137$ s.
$\tau_{complex} = 348$, s. $\zeta = .44$
$\tau_{complex} = 140$, s. $\zeta = .44$

evaluated at $Q_i/Q_x = .54$, $R_i = 2$ cm, and $T_b = +84$ K.

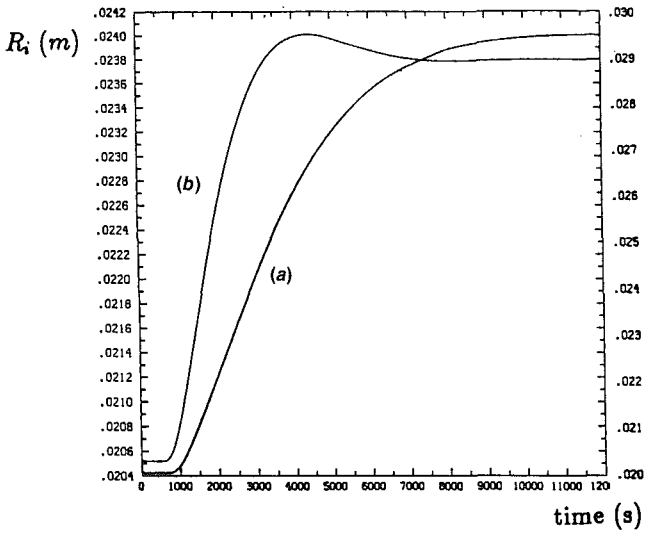

Fig. 3 R_i response to step decrease in heater power: $\delta P_{in}/P_{in} = 0.05$, (a) $Q_i/Q_x = .54$, (b) $Q_i/Q_x = .34$

$H_m = 6$ cm, $R_i = 2$ cm, $V_p = 3 \times 10^{-5}$ m/s (10.8 cm/hr). The system is dominated by a real pole that is 5 times slower than the most dominant complex pair. Even though the damping ratio of the complex poles is fairly low ($\zeta = .46$), the separation from the slower real poles is large enough to mask out the contribution of the complex poles. This effect is illustrated in the response to a step decrease in heater power shown in Fig. 3, curve (*a*). (The nonlinear model is used for all simulations.)

One interesting feature of the ILOM that seems to contradict results of the flat-interface low order model (Gevelber and Stephanopoulos, 1987) is that the interface diameter dynamics is well damped in spite of the low ratio of the melt-interface heat flux, Q_i to the crystal heat flux, Q_x. Previously we showed that the eigenstructure of the interface becomes poorly damped as Q_i/Q_x becomes small. The ILOM, also displays the behavior of being more oscillatory as the ratio of Q_i/Q_x decreases as shown in Fig. 3. As predicted by our previous analysis (Gevelber and Stephanopoulos, 1987), the additional degrees of freedom for the interface shape in the ILOM results in the fact that there is a decrease in the oscillatory nature of the response. (In the flat interface model, some oscillations are observed even at $Q_i/Q_x = .8$, Gevelber and Stephanopoulos, 1987). The reason is that the separation between the complex and real pole increases as more degrees of freedom are added to the interface model. This is consistent with the experimental step response results observed by Wargo and Gevelber. These experiments were conducted for $R_i/R_{cru} \ll 1$ in order to observe the interface response under quasi-steady state conditions, i.e., minimizing the melt height ramp disturbance effects (see next section). In these experiments, no oscillatory behavior was observed for step changes in pulling rate of ± 25 percent.

Another test of model accuracy was made by comparing the predicted and actual temperature changes in the heater and crucible for a step change in heater power. Figure 4 shows that the model matches the dynamic response of the physical system fairly well.

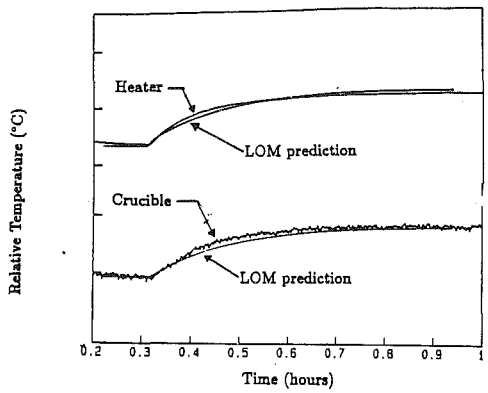

Fig. 4 Comparison of predicted and actual heater and crucible temperatures to a step increase in power

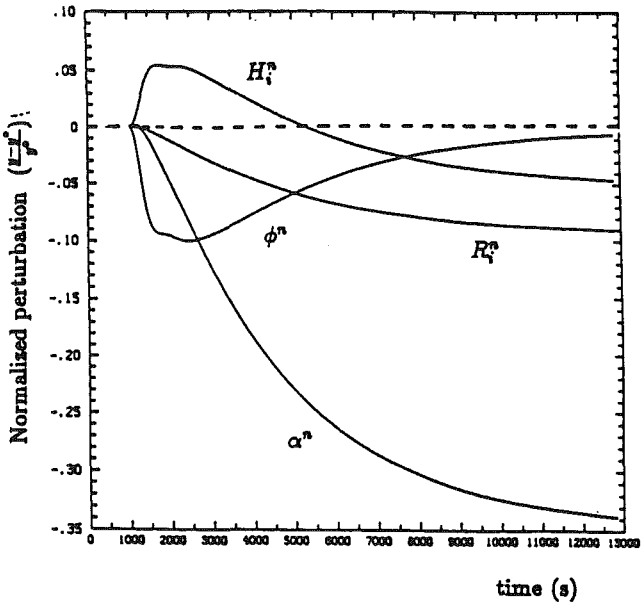

Fig. 5 Normalized perturbation responses to a step increase in heater power for R_i^n, $5H_i^n$, ϕ^n, α^n where $y^n = (y - y^0)/y^0$

Dynamic simulation and eigenstructure analysis reveals that several interface shape parameters have right half plane (RHP) zeros. Figure 5 shows the response to a step increase in heater power for R_i, H_i and ϕ. The interface height, H_i, shows the characteristics of a RHP zero and is the cause of the weight measurements "anomalous" effect (Bardsley et al., 1977). The problem stems from the fact that the weight cell measures the hydraulic head of the meniscus that attaches to the crystal in addition to the crystal weight. Thus, in semiconductor systems where the density of the liquid is greater than the solid, the weight measurement first increases with H_i even though R_i is decreasing. Experimentally, this effect was observed, and although the physical cause identified by Bardsley et al. in 1977, its significance in terms of achievable control performance was not understood until it was identified as a RHP zero (Gevelber et al., 1988). It can be shown that the RHP zero imposes a fundamental limitation on achievable control performance (Freudenberg and Looze, 1986). In addition, the RHP zero also limits the estimation accuracy to infer other important variables (Gevelber et al., 1988). Thus, if the control system needs to have good disturbance rejection and command performance at frequencies above the RHP zero, the weight measurement should not be used.

The dynamic response for the interface angle θ_i shows that it also has a RHP zeros (Fig. 6). Analysis of the linearized state equations reveals that this is true for δH as well (Table

Table 2 Dominant right half plane SISO zeros

	P_{in}	V_p	T_{men}	T_{bot}
R_i	—	—	—	—
∂H	$.0052 \pm .0053j$	.0034	.00076	$.0052 \pm .0053j$
θ_i	$.004 \pm .007j$	.0036	.0007	$.004 \pm .007j$

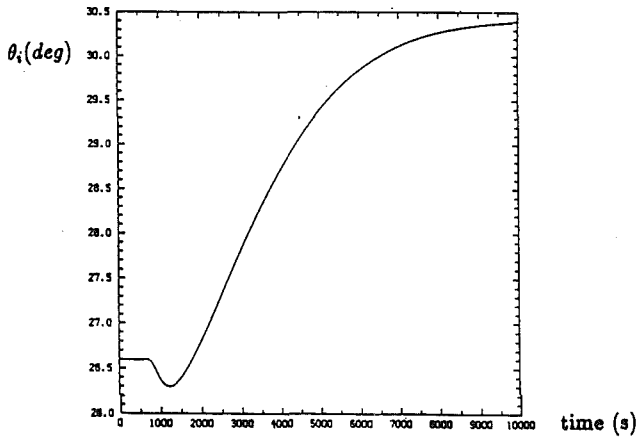

Fig. 6 θ_i response to step decrease in power for $Q_i/Q_x = .54$

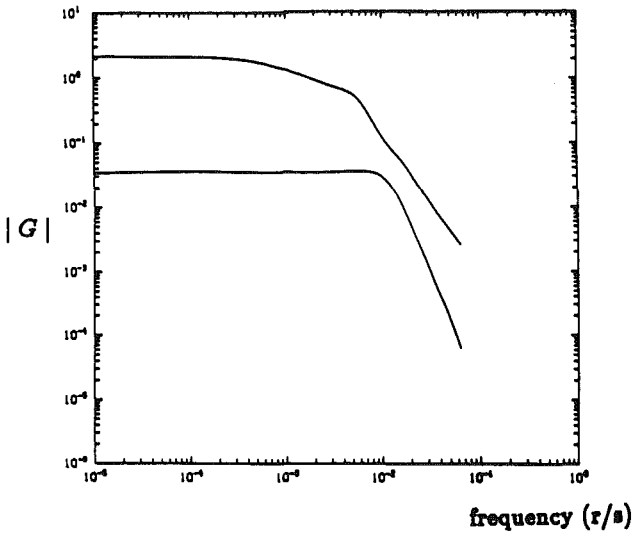

Fig. 7 SVD frequency plot for LOM: y: R_i, θ_i u: P_{in}, V_p

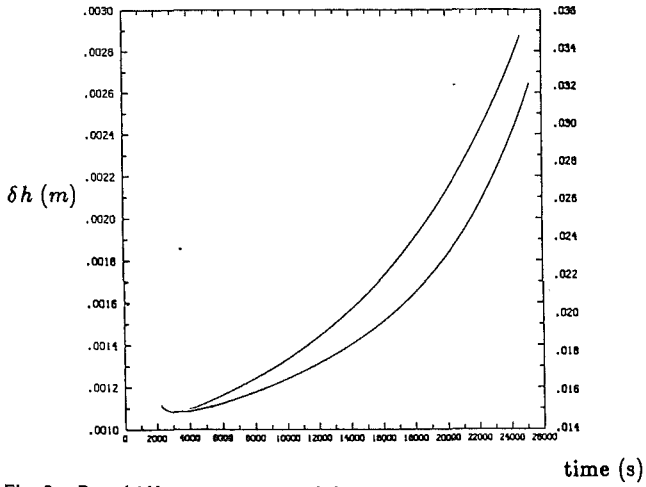

Fig. 8 R_i and δH responses to melt height drop with adiabatic bottom

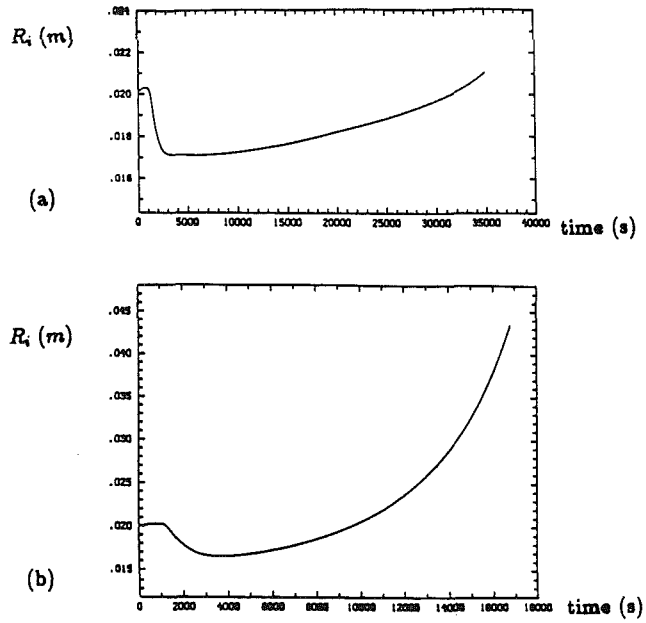

Fig. 9 R_i response to melt height drop: (*a*) heated bottom ($T_{\text{bot}} = +110$ K), and (*b*) cooled bottom ($T_{\text{bot}} = -84$ K)

2 lists the dominant zeros for different inputs). These zeros pose a more serious problem since they are associated with the physical variables that are important to control. The performance implication is that if one tries to separately control either δH or θ_i, there will be a fundamental limitation on the achievable performance.

There is no RHP zero problem however, in considering the multivariable control problem. Analysis of the MIMO system of $\mathbf{y} = (R_i, \theta_i)$, $\mathbf{u} = (P_{\text{in}}, V_p)$ where $\mathbf{y} = G(s)\mathbf{u}$ shows the system does not have a corresponding RHP transmission zero. This is true for all other pairings of the inputs. The significance is that the MIMO system will not be faced by the fundamental performance limitation that the SISO systems will face. From a control viewpoint, MIMO control of R_i, θ_i results in a better posed operating regime, but at the expense of increasing the complexity of the controller.

The Bode magnitude plots between R_i and the conventional inputs, P_{in}, V_p, reveal that the pull rate input has a greater bandwidth than the heater power (Gevelber et al., 1988). Thus, use of heater power input might result in poorer performance. The problem with use of pull rate input, however, is that it might induce a disturbance into the mass transport. Bode plots, however, do not provide insight as to the effect of cross coupling between channels. To analyze these effects, a singular value decomposition (SVD) must be made.

The SVD provides information about the minimum and maximum "amplification" power of a matrix in mapping vectors. They are used to calculate the norm a matrix, represented $\|\cdot\|$. The norm of a matrix gives a measure of the maximum "amplification" power. For a matrix A, where $\mathbf{b} = A\mathbf{x}$, $|\mathbf{b}| \le \|A\| |\mathbf{x}|$. The norm of the matrix is calculated by the singular value decomposition. The maximum and minimum singular values of a matrix, denoted $\bar{\sigma}$, $\underline{\sigma}$, represent the maximum and minimum "amplification power" of the matrix such that $\underline{\sigma}(A)|\mathbf{x}| \le |\mathbf{b}| \le \bar{\sigma}(A)|\mathbf{x}|$. Thus, $\|A\| = \bar{\sigma}(A)$.

The singular values of the MIMO system are sensitive to the scales selected for the inputs and outputs. Typically, they are nondimensionalized and scaled to reflect their operational ranges. A large ratio of the maximum to minimum singular value, known as the euclidean condition number κ_2, indicates the possibility of adverse coupling between the inputs and outputs. Figure 7 shows the SVD frequency plot for outputs R_i, θ_i for the conventional inputs P_{in}, V_p. Even at DC, $\kappa_2 = 16$.

3.1 Batch Effects. Gevelber and Stephanopoulos (1987) showed that the changed melt height level acts as a disturbance to the growth dynamics due to the decreasing heat transfer area between the crucible and the melt. When a separate crystal

thermal environment is used, which eliminates heat transfer between the crystal and hot crucible wall, the crystal diameter increases since the melt temperature decreases. In a conventional system, the specific effect of the disturbance may be different since there is also the interaction from the crucible to the crystal. For all systems, the melt disturbance affects the interface deflection and the eigenstructure in addition to the diameter. The change in eigenstructure is important since a large change might require special compensation, especially since MIMO controllers entail more difficult robustness problems.

Figure 8 shows the change of R_i and δH as the melt level decreases throughout the batch cycle. The deflection changes both because the diameter is increasing but also due to the change of heat flux conditions as the melt level gets closer to the bottom. As Derby and Brown (1986) have shown, the heat transfer condition of the crucible bottom (i.e., whether it's adiabatic, a heat source, or sink) significantly affect this result.

Bottom heaters are now available for commercial pullers although there is little documentation as to how they should be used in the growth cycle. Derby and Brown (1986b) calculated feedforward trajectories for bottom heaters to maintain a desired interface deflection, while Cazin-Bourguignon and Motakef (1989) shows their effect on the thermal stress of the growing crystal. From a control point of view, it is desirable to analyze the effect of bottom heaters on the eigenstructure of the system and its effect on the achievable operating regime.

Three alternative bottom thermal conditions are considered: (*a*) adiabatic bottom, (*b*) heated bottom, (*c*) cooled bottom. The modeling presented here actually covers the conventional practice which corresponds to case (*c*) since heat in a conventional system heat is typically lost through the bottom of the crucible to the water cooled support shaft. Condition (*a*) is modelled by considering no heat input to the bottom of crucible elements while conditions (*b*) and (*c*) are modeled by assuming that the temperatures at the bottoms of those elements are proportional to a specified differences from interface temperature.

The crucible bottom heat transfer condition has a profound effect on the batch disturbance on the crystal diameter and interface deflection. Figures 8 and 9 show the different responses to the melt height drop for the three cases. Heat loss from the crucible bottom exacerbates the decrease in melt temperature due to the melt level decrease, causing the crystal to grow out faster. Crucible bottom heat loss can in fact have a greater effect than the melt height drop since the area for the bottom loss is proportional to the square of the crucible radius, whereas the melt height effect is only proportional to the crucible radius. Heating the crucible bottom counters the decrease of heat due to the melt height drop (Fig. 9, curve (*a*)). Thus, use of a hot bottom minimizes the disturbance effect of the melt height decrease. Heating the bottom when there is an independent crystal thermal environment does not tend to deflect the interface out as in the case of the conventional system (Derby and Brown, 1986b and Motakef, 1989). The choice of bottom thermal boundary condition also affects the dynamics of the process. The system with a heated bottom is significantly faster (2172 seconds for the dominant pole) than either the cooled (5200 seconds) or adiabatic bottom (9600 seconds).

4 Summary

To analyze the issues associated with controlling interface shape, a low order model is developed that captures the important process physics, input/output coupling, and disturbances. Specific features include interface shape and system temperature gradients, as well as a number of alternative actuators including magnetic field, bottom heaters, special thermal actuators for the crystal, pull rate, and main heaters. Simulation of the interface dynamic response and determination of the transfer functions reveal that the interface angle and deflection have RHP zeros. This poses an inherent performance limitation since it's related to the control objective and not just to the measurement technique. Thus, if these variables were to be independently controlled there would be a fundamental limitation on achievable performance. The specific control objectives and control design of the coupled outputs will be evaluated in the companion paper.

Acknowledgments

The authors would like to thank M. J. Wargo, S. Motakef, R. A. Brown and A. F. Witt for discussions related to this work, and to DARPA and the U.S. Air Force for financial support.

References

Borodin, V. A., Davidova, L. B., Erofeev, V. N., Shdanov, A. V., and Strartsev, S. A., 1979, "The Effect of the Solidifcation Front Shape on the Temperature Distribution in the Crystal," *J. Crystal Growth*, Vol. 46, p. 757.

Bardsley, W., Cockayne, B., Green, G. W., Hurle, D. T. J., Joyce, G. C., Roslington, J. M., Tufton, P. J., and Webber, H. C., 1974, "Developments in the Weighing Method of Automatic Crystal Pulling," *J. Crystal Growth*, Vol. 24/25, p. 369.

Brice, J. C., Hill, O. F., Whiffin, P. A. C., and Wilkinson, J. A., 1971, "The Czochralski Growth of Barium Strontium Niobate Crystals," *J. Crystal Growth*, Vol. 10, p. 133.

Cambridge Instruments, 1986, "Multiple Heaters for the LEC Growth of III-V Compounds."

Cazin-Bourguignon, A-M., and Motakef, S. J., 1989, "Thermoelastic Analysis of GaAs in LEC Growth Configuration. III Effectiveness of Top Assembly and Bottom Heaters in Control of Stresses in Low Pressure Systems," *J. Crystal Growth*, Vol. 96, p. 390.

Derby, J. J., and Brown, R. A., 1986b, "Thermal-Capillary Analysis of Czochralski and Liquid Encapsulated Czochralski Crystal Growth, II. Processing Strategies," *J. Crystal Growth*, Vol. 75, p. 227.

Ekhult, U., and Carlberg, T., 1986, "Czochralski Growth of TIN Crystals Under Constant Pull Rate and IR Deameter Control," *J. Crystal Growth*, Vol. 76, p. 317.

Freudenberg, J. S., and Looze, D. P., 1985, "Right Half Plane Poles and Zeros and Design Tradeoffs in Feedback Systems," *Automatic Control*, Vol. AC-30, No. 6, p. 555.

Gevelber, M. A., and Stephanopoulos, G., 1987, "Dynamics and Control of the Czochralski Process, I. Modelling and Dynamic Characterization," *J. Crystal Growth*, Vol. 84, p. 647.

Gevelber, M. A., Stephanopoulos, G., and Wargo, M. J., 1988, "Dynamics and Control of the Czochralski Process, II. Objectives and Control Structure Design," *J. Crystal Growth*, Vol. 91, p. 199.

Hurle, D. T. J., Joyce, G. C., Wilson, G. C., Ghassempoory, M., and Morgan, C., 1986, "A Technique for Experimentally Determining the Transfer Function of a Czochralski Pulling Process," *J. Crystal Growth*, Vol. 74, p. 480.

Jasinski, T., and Witt, A., 1986, "Apparatus for Growing Crystals," U.S. patent 4,597,949.

Kobayashi, T., Kohda, H., Nakanishi, H., Hyuga, F., and Hoshikawa, K., 1986, "VM-FEC Growth for High Quality, Large Size, Dislocation Free GaAs Crystals," *Semi-Insulating III-V Materials*, p. 17.

Motakef, S., 1989, "Thermoelastic Analysis of GaAs in LEC Growth Configuration. III Thermal Conditions for Control of Stresses in Low Pressure Systems," *J. Crystal Growth*, Vol. 96, p. 201.

Robertson, D. S., and Young, I. M., 1975, "Observations on the Unrestrained Growth of Germanium Crystals," *J. Phys. D: Appl. Phys.*, Vol. 8, p. 38.

Sackinger, P. A., 1988, "Mechanisms for Flow During Czochralski Si Growth," Seminar, MIT, May 12.

Srivastava, R. K., Ramachandran, P. A., and Dudukovic, M. P., 1985, "Interface Shape in Czochralski Grown Crystals: Effect on Conduction and Radiation," *J. Crystal Growth*, Vol. 73, p. 487.

Steel, G. K., and Hill, M. L., 1975, "Analysis of the Transfer Function Governing Crystal Growth in the Czochralski Process," *J. Crystal Growth*, Vol. 30, p. 45.

Juhasz, Z., and Szabo, G., 1986, "Fluctuations of Melt Temperature and Growth Rate During $Bi_4Ge_3O_{12}$ Growth," *J. Crystal Growth*, Vol. 79, p. 303.

Tangborn, A. V., 1987, "Numerical Simulations of Czochralski Bulk Flows," Ph.D. thesis, Department of Mechanical Engineering, M.I.T.